Glaucoma

Time–Frequency Analysis of ERG With Discrete Wavelet Transform and Matching Pursuits for Glaucoma

Marc Sarossy[1], Jonathan Crowston[2], Dinesh Kumar[3], Anne Weymouth[4], and Zhichao Wu[1,5]

[1] Ophthalmology, Department of Surgery, University of Melbourne, Melbourne, Victoria, Australia
[2] Duke-NUS Medical School, Singapore
[3] RMIT University, Melbourne, Victoria, Australia
[4] Department of Optometry and Vision Sciences, University of Melbourne, Melbourne, Victoria, Australia
[5] Centre for Eye Research Australia, Royal Victorian Eye and Ear Hospital, East Melbourne, Victoria, Australia

Purpose: To examine the performance of two time–frequency feature extraction techniques applied to electroretinograms (ERGs) for the prediction of glaucoma severity.

Methods: ERGs targeting the photopic negative response were obtained in 103 eyes of 55 patients with glaucoma. Features from the ERG recordings were extracted using two time–frequency extraction techniques based on the discrete wavelet transform (DWT) and the matching pursuit (MP) decomposition. Amplitude markers of the time-domain signal were also extracted. Linear and multivariate adaptive regression spline (MARS) models were fitted using combinations of these features to predict estimated retinal ganglion cell counts, a measure of glaucoma disease severity derived from standard automated perimetry and optical coherence tomography imaging.

Results: Predictive models using features from the time–frequency analyses—using both DWT and MP—combined with amplitude markers outperformed predictive models using the markers alone with linear ($P = 0.001$) and MARS ($P \leq 0.011$) models. For example, the proportions of variance (R^2) explained by the MARS model using the DWT and MP features with amplitude markers were 0.53 and 0.63, respectively, compared to 0.34 for the model using the markers alone ($P = 0.011$ and $P = 0.001$, respectively).

Conclusions: Novel time–frequency features extracted from the photopic ERG substantially added to the prediction of glaucoma severity compared to using the time-domain amplitude markers alone.

Translational Relevance: Substantial information about retinal ganglion cell dysfunction exists in the time–frequency domain of ERGs that could be useful in the management of glaucoma.

Introduction

Glaucoma is an optic neuropathy characterized by the progressive loss of retinal ganglion cells (RGCs),[1] which exhibit structural and functional changes prior to their death by apoptosis.[2] Early RGC structural changes include reduction in the length and number of dendrites and the area of the dendritic arbor, as seen from mouse models of optic nerve injury.[3,4] Functional changes in the RGCs prior to apoptosis can include an increased firing rate from increased excitability[5,6]

and a fall in the mean and peak spike rates.[7] Detecting these early functional changes might potentially aid the prediction of future RGC loss in glaucoma and thus enhance the clinical management of progression of this condition, which was estimated to affect 64.3 million people in the world between the ages of 30 and 80 years in 2013.[8]

Electrophysiological recordings from the eye may be able to detect the earliest changes in RGC function. In a study on glaucoma suspects, Banitt et al.[9] showed that a 10% change in the pattern electroretinogram (PERG) amplitude preceded the same change in

peripapillary retinal nerve fiber layer (RNFL) thickness by 8 years. Liu et al.[10] worked in a rat model and showed that, with chronic intraocular pressure (IOP) elevation, the positive scotopic threshold response was reduced by 25% in animals with elevated pressure without any changes in the optical coherence tomography (OCT) parameters and that these changes reversed with normalization of the IOP. It is therefore plausible that the electroretinogram (ERG) is a tool that could be used to capture such early functional abnormalities of the RGCs. The ERG is a time-domain signal of the electrical activity of the retina in response to light stimuli. When recorded under light-adapted conditions with a brief presentation of a red-on-blue stimulus, a slow negative going wave occurring after an initial a-wave trough and b-wave peak—termed the photopic negative response (PhNR)—is typically observable.[11] The PhNR is a response that arises from the RGCs and has been demonstrated to be reduced in glaucoma, both in experimental models and in clinical studies.[12–17] It can show improvement in patients with glaucoma when the IOP is lowered[18] and has been used as a marker of inner retinal function in patients with glaucoma when treated with nicotinamide.[19] The signal between the b-wave peak and the PhNR trough is frequently interrupted by the i-wave, which is thought to arise from the cells distal to the RGCs.[20] If the i-wave is present, the PhNR can be recorded as either the negative wave between the b-wave and i-wave (the PhNR1) or the negative wave following the i-wave (the PhNR2). We have previously shown that a combination of key amplitude markers of the ERG—namely, the a-wave, b-wave, i-wave, and PhNR (PhNR1 and PhNR2) amplitudes—better predicts glaucoma severity than the PhNR amplitude alone.[21] These findings underscore how a photopic ERG contains more information about RGC function than is captured by conventional PhNR measures alone.

The ERG measured from a single differential pair electrode is a mixture of the underlying processes, which occur at different times after the stimulus.[22] The underlying mechanisms are complex[23] with feedback[24] and feedforward pathways,[25,26] and there are slow and fast frequency components from the different sources of the signal. Time–frequency analysis has the potential to extract these components from the photopic ERG to provide further insights into RGC function, above and beyond what is captured by the amplitude markers of the ERG. With time–frequency analysis, a vector of amplitude measurements is transformed into a matrix of coefficients with axes of time and frequency so that the magnitude and timing of frequency components within the signal can be determined. The wavelet transform, a form of time–frequency analysis, has been

described as an alternative to short-time Fourier transform.[27,28] A wavelet is a small function (little wave) that acts as a filter and can localize energy within the signal in time and frequency. This is achieved through multiplication of the signal and wavelet after translation and dilation of the wavelet relative to the signal for time and frequency resolution, respectively. Wavelets have been applied to the PERG,[29] multifocal ERG,[30] and photopic ERG[31] in the assessment of glaucoma.

There are two types of wavelet transforms: continuous wavelet transform (CWT)[28] and discrete wavelet transform (DWT).[32]

The CWT is obtained by convoluting the wavelet with the signal for all values of scale (e.g., frequency) and time lag, creating a continuous scalogram showing the energy of the signal at each frequency and time point. However, this creates a highly redundant output matrix, as both its width and length are now equal to the number of samples in the original time series vector. Forte and colleagues[33] showed that the Morlet wavelet could be used to isolate oscillatory potentials in rat ERGs. Behbahani and colleagues[34] used a Mexican hat wavelet to determine the dominant frequencies associated with the PhNR in patients with central retinal vein occlusion and found that the dominant frequency decreased. However, the CWT has not thus far found clinical utility for glaucoma.

On the other hand, the DWT[32,35,36] uses set scales and time lags at discrete values, where the output is in the form of a binary tree and the total number of coefficients is equal to the number of samples in the input, which necessarily must be of length equal to a power of two. Specifically, it uses a low-pass filter (scaling function) and a high-pass filter (wavelet function), followed by downsampling by two. There are many mother wavelets available for the DWT. Selection of the mother wavelet optimizes the resolution in time and frequency for the temporal and spectral content of the signal. Various techniques for mother wavelet selection have been described,[37] including minimizing informational cost. The DWT has been applied to glaucoma, but previous studies have generally used a single feature derived from the transform.[30,38] A recent paper explored the use of the DWT in the photopic ERG and found differences between individuals diagnosed with autism spectrum disorder compared with control subjects.[39]

A different approach to time–frequency analysis is the matching pursuit (MP) algorithm.[40] The MP algorithm decomposes a time-domain signal into a linear combination of subsignals of the same length termed atoms. The full set of atoms is referred to as the dictionary. The decomposition output is a set consisting of a coefficient for each atom in the

dictionary. The process of generating the dictionary usually begins with a discrete wavelet family: small vectors representing digital filters.[32] In contrast to the DWT, the atoms in the MP decomposition are padded to the length of the signal rather than a much shorter vector that slides along the signal. The dictionary thus includes all of the time shifts of a given wavelet as separate atoms. The algorithm process is known as "greedy." It starts by finding the best match to the signal from the entire dictionary, removes that part of the signal, and then finds the next best match and so on. The number of iterations is usually equal to the length of the dictionary, although a smaller fixed number can be used, or the algorithm can reach a stopping criterion. The result of the transformation is the coefficient for each atom and the index into the dictionary used. The dimensionality of the transformation may be larger or smaller than the original signal.

We therefore posed this optimization problem: Given a continuous outcome measure (the estimated RGC), can additional features extracted by the DWT or the MP informing linear or MARS models yield better performance than time-domain amplitude features alone? Although the DWT is more straightforward for others to replicate with widely available software, the MP technique may offer better time localization for low frequencies. Some studies have compared the two techniques in hyperspectral imaging[41] and electroencephalogram analysis,[42] although these studies addressed classification rather than regression problems and the differences were modest. Both techniques in theory allow the extraction of multiple features from the underlying processes and could plausibly better characterize the extent of retinal dysfunction than time-domain features alone.

Given the ability of the DWT and MP algorithms to extract novel time–frequency features from the photopic ERG, we examined whether these approaches, when used together with an extended set of amplitude markers, could be used to better predict glaucoma severity (or the extent of RGC loss and dysfunction). We compared the incremental benefit of each method and the combination of both. Our aim was not to develop a new clinical tool for the diagnosis of glaucoma or the classification of its severity, as clinicians currently have OCT, standard automated perimetry (SAP), and clinical examination for that. Rather, the aim of this study was to elucidate additional information within the ERG that can be extracted by time–frequency techniques and which might ultimately be useful in, for example, building a predictive model of progression.

Methods

This study was an approved study by the Human Research Ethics Committee of the Royal Victorian Eye and Ear Hospital, and it was conducted in accordance with the tenets of the Declaration of Helsinki. All participants provided written informed consent prior to any study procedures being undertaken.

Participants

Participants with primary open-angle glaucoma were recruited from a private ophthalmology practice, and the diagnosis of glaucoma was based on a comprehensive clinical assessment by an ophthalmologist based on characteristic optic nerve head appearance, the presence of glaucomatous visual field defects, and/or neuroretinal tissue loss on OCT imaging. Participants with ocular or systemic diseases that could affect the optic nerve (such as choroidal neovascular membrane, extensive macular atrophy, diabetic retinopathy, multiple sclerosis, or epiretinal membrane) were excluded. Only individuals over the age of 18 were eligible. Both eyes were included where glaucoma was bilateral, and only eyes with an acuity of 20/40 (or 0.30 logMAR) or better were included in this study.

Automated Perimetry

All participants performed SAP testing using the 24-2 Swedish interactive thresholding algorithm (SITA) Fast protocol on the Humphrey Field Analyzer 3 (Carl Zeiss Meditec, Jena, Germany), following correction of the spherical refractive error component from subjective refraction. Only visual field results where fixation losses or false-negative responses were ≤33% and false positive responses were ≤20% were considered reliable and analyzed in this study.

Optical Coherence Tomography

All participants underwent optic disc-centered OCT volume scans performed with the CIRRUS HD-OCT device (Carl Zeiss Meditec) with dilated pupils. Each scan consisted of 200 × 200 A-scans and covered an area of 6 × 6 mm. The global circumpapillary RNFL thickness scan was calculated from a derived 3.46-mm-diameter circle scan consisting of 256 A-scans. All scans were checked for centration and segmentation accuracy.

Estimated RGC Counts

For each eye, the measure of estimated RGC (eRGC) counts, as described by Medeiros and colleagues,[43] was derived to provide an index of disease severity. This measure was based on empirical formulas developed by Harwerth and colleagues[44] in non-human primates, which related RGC counts to visual field measurements. In brief, the eRGC is based on an estimate of the number of RGC somas in each retinal region sampled on SAP (SAP_{rgc}) and also an estimate of the number of RGC axons at the circumpapillary circle on OCT imaging (with corrections for the effects of disease-related remodeling of the RNFL axonal and non-axonal composition, or OCT_{rgc}). Medeiros and colleagues[43] proposed the use of a weighted mean of the structural and functional estimates to reflect the inverse relationship between the accuracies of clinical SAP and OCT imaging estimates with disease severity. Using the mean deviation (MD) values from SAP as a measure of disease severity, the eRGC count in an eye was thus calculated as

$$\mathrm{eRGC} = \left(1 + \frac{\mathrm{MD}}{30}\right)\mathrm{OCT}_{rgc} - \frac{\mathrm{MD}}{30}\mathrm{SAP}_{rgc} \quad (2)$$

A recent paper found the range of the eRGC in healthy eyes without glaucoma to be $1{,}102{,}108 \pm 72{,}669$.[45]

ERG Recordings

An Espion E3 system (Diagnosys, Lowell, MA) was used with a Diagnosys ColorDome light-emitting diode Ganzfeld stimulator to collect the ERG data. The recordings were in compliance with the International Society for Clinical Electrophysiology of Vision (ISCEV) 2018 extended protocol for the photopic negative response of the electroretinogram.[11] Participants were not dark adapted at any stage of the testing. They were adapted to ambient light in the testing suite for at least 10 minutes during pupil dilation. Both eyes were dilated with 1% tropicamide drops prior to recording, and active Dawson–Trick–Litzkow electrodes were used with gold-cup skin electrodes as the reference and ground electrodes. The ground electrode was placed at Fz and the reference electrode at the lateral canthus. Impedances of all electrodes, including the ground, were checked to ensure that they were less than 5 kΩ. The stimulus parameters were compliant with the protocol and used a blue background of 10 cd/m^2 (peak wavelength = 465 nm) with a preadaptation time within the Ganzfeld dome of 2 minutes and presenting red flashes (peak wavelength = 635 nm) with a 4-ms duration at 1 cd·s/m^2. A sample rate of 4000 Hz was used with 20 ms of pre-stimulus

and 250 ms of post-stimulus recording, yielding a vector length of 1079 samples. Flashes were presented at 2 Hz. Voltage-based automatic rejection of traces with blink or movement artifacts was used[17,46] with signals with an absolute amplitude of 200 μV within 100% of the sweep range rejected. This value replicated the level used in our laboratory for routine photopic full-field electroretinogram recordings with this equipment and electrode type. A total of 125 unrejected sweeps per stimulus were collected. Bandpass filtering from 0.3 to 100 Hz was performed. This upper bound, which is lower than the high-frequency cutoff of the ISCEV protocol, was chosen as the pilot for this project used a achromatic stimulus and the standard photopic ERG protocol of the laboratory.

Preprocessing

After signal averaging of the unrejected traces, the ensemble averages were trimmed so that the b-wave peak occurred at the 200th sample and the epoch was 1024 samples long. The alignment process is illustrated in Figure 1. The alignment was performed because the region of interest within the time–frequency spectrum is much later than for analysis of outer retinal function via traditional electroretinogram markers. Aligning the averages in this way ensures that the largest coefficient of either the DWT or the MP corresponds in all cases to the b-wave.

Amplitude Markers

For each ensemble average of ERG traces, amplitude markers were determined as described previously.[21] Briefly, the a-wave trough was determined as the first negative trough after the stimulus onset, and the b-wave peak was found as the first peak after the a-wave. The i-wave was found as the first peak or inflexion point after the b-wave. The PhNR1 was the first trough between the b-wave and the i-wave, or equal to the i-wave in the case of that being an inflexion point. The PhNR2 was found as the first trough after the i-wave.

Discrete Wavelet Transform

For each trace, the DWT was performed using Wavelet Methods for Time-Series Analysis (WMTSA) version 2.0-3 in R (R Foundation for Statistical Computing, Vienna, Austria).[47] Figure 2 shows a typical ERG and the DWT performed in this case with a Daubechies wavelet with 8 vanishing moments (d8 wavelet), with the heatmap showing the absolute magnitude of the wavelet coefficients by decomposition level and position in time.
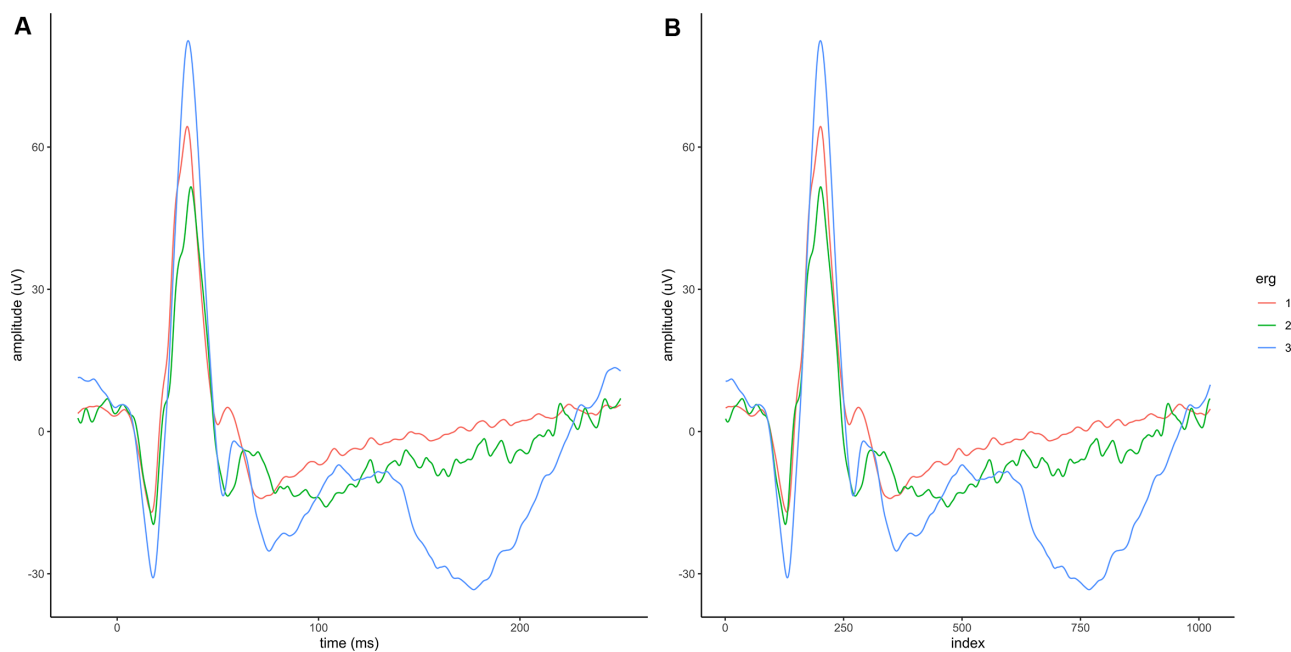
Figure 1. Alignment of the traces. Three ERG ensemble averages are illustrated. (A) Original traces plotted against post-stimulus time. (B) Alignment of the traces so that the b-wave peak occurs at sample 200 of 1024.
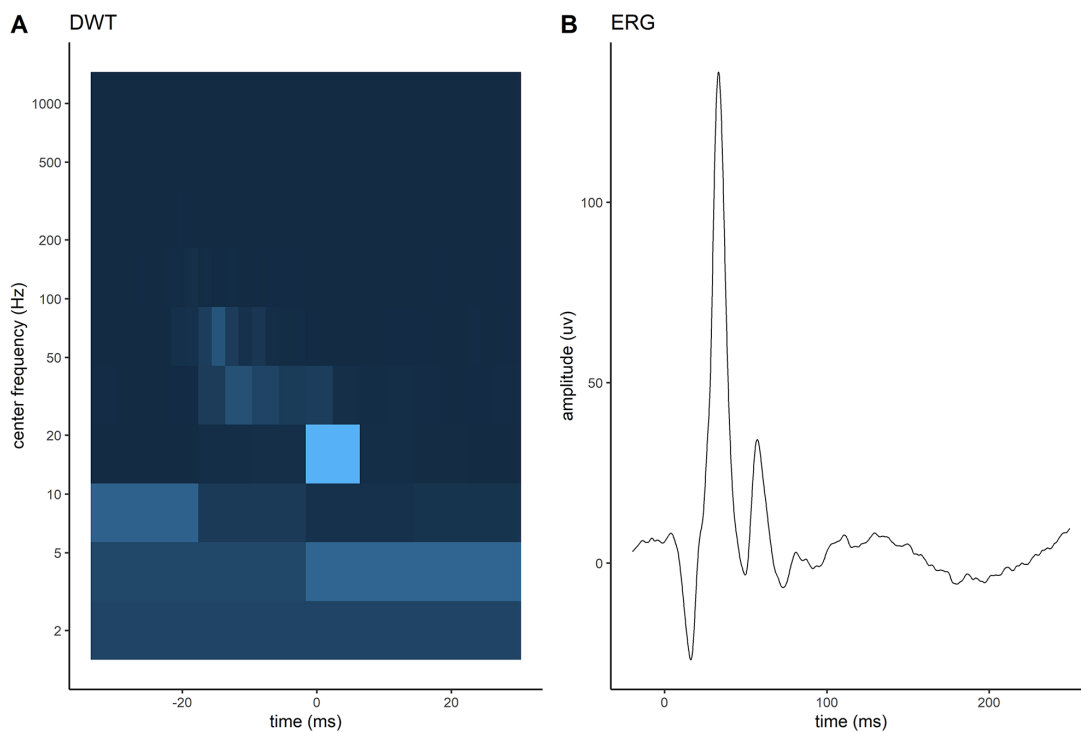

Figure 2. DWT of the ERG. (A) Magnitude of the detail coefficients of the DWT (scalogram). (B) ERG as a function of amplitude relative to time.
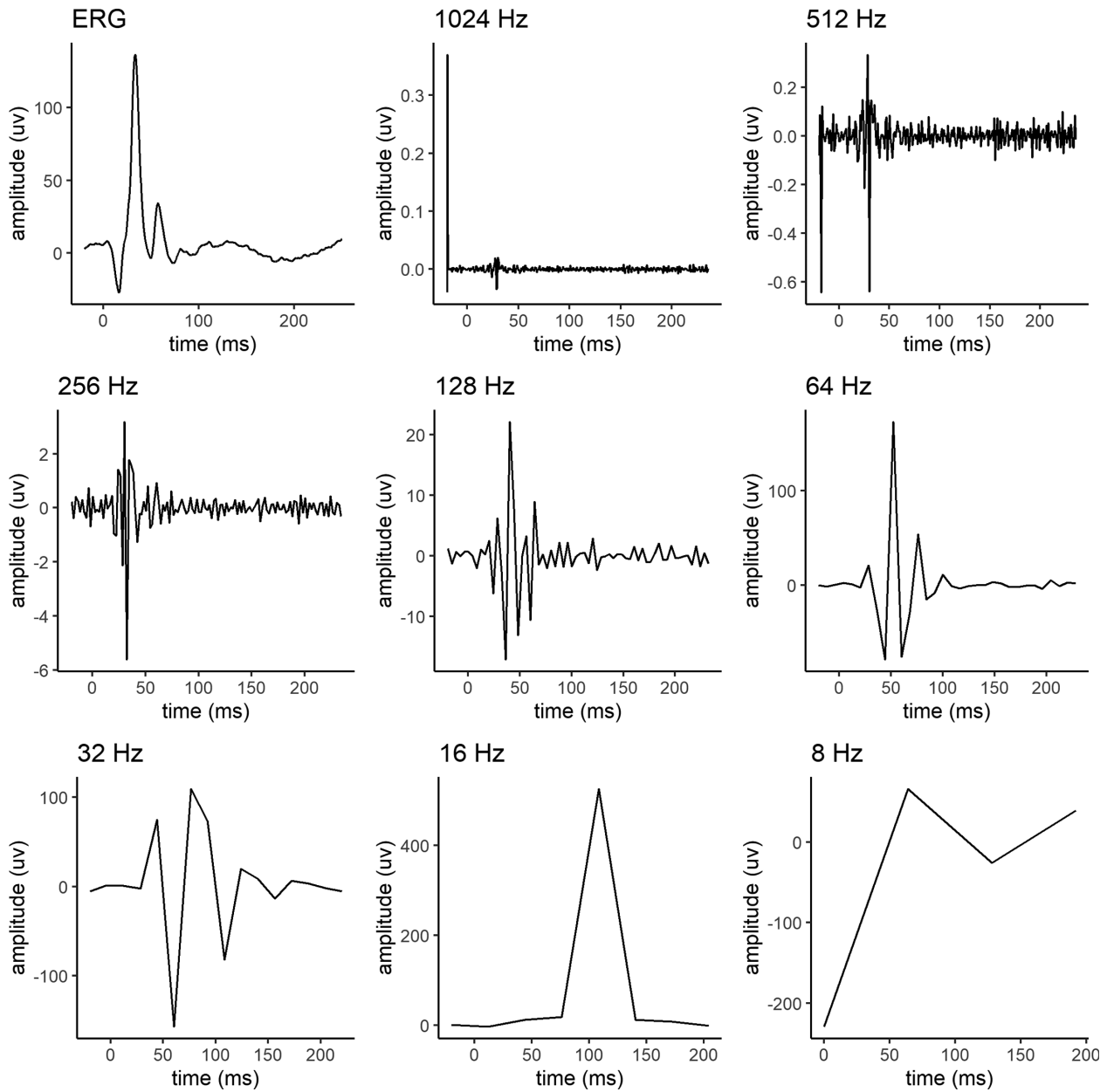
Figure 3. DWT decomposition of the ERG by level. The first panel represents the time-domain signal. Each subsequent panel shows the detail coefficients plotted on a horizontal axis scaled to the same length as the original time-domain signal. The panel label shows the center frequency of the wavelet. At the first decomposition level, the length of the signal is reduced by half and so on for each subsequent decomposition level.

Figure 3 shows each decomposition of the waveform presented in Figure 1 by the DWT, with the magnitude retaining the sign information. The horizontal axis of each subplot has been scaled to retain the same overall width for comparison.

The list of wavelets examined in this study includes the Coiflet, Symlet, Daubechies, and Best Localized wavelets over all available vanishing moments. These wavelets differ in terms of orthogonality (the extent to which the coefficients are correlated), symmetry (which provides linear phase), compact support, and

filter order (an increased filter order of the mother wavelet increases smoothness).[48] Optimal wavelet selection was performed by minimizing the ratio of energy to Shannon entropy.[49] The energy for each wavelet was calculated by the sum of all the wavelet coefficients squared. The Shannon entropy was calculated by the plug-in estimator[50] for all of the coefficients over 20 bins. The plug-in estimator is a technique for estimating the entropy by using the empirically measured frequencies of the bins to directly estimate the probabilities used in the calculation. That is, $\hat{H} = -\sum_k \widehat{p_k} ln \widehat{p_k}$,
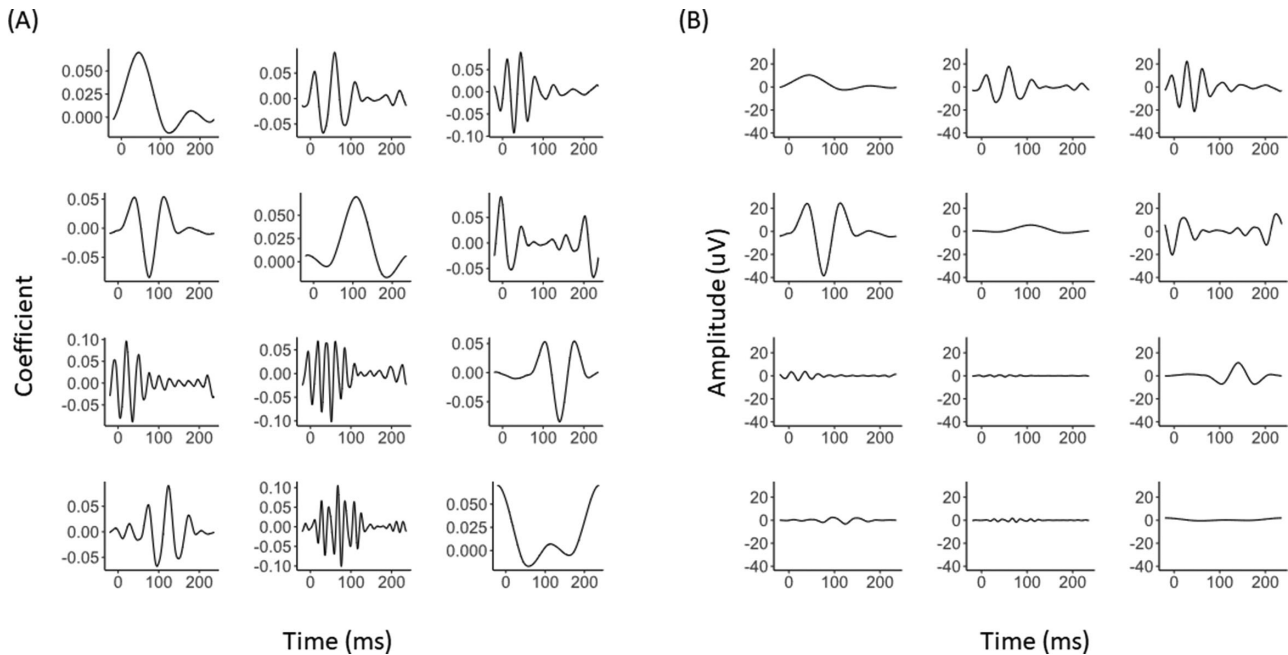
(A)

(B)

Figure 4. Sample matching pursuit decomposition. (A) The dictionary of atoms used for the decomposition and the coefficients for each, and (B) the atoms multiplied by the coefficient. Note that some of the coefficients are negative; the upper right trace of (A) has been inverted in (B). The decomposition consists of the coefficients for each atom in the dictionary.

where $\hat{H}$ is the estimated entropy for the k bins, and $\widehat{p_k}$, the estimated probability for the kth bin, is given simply by the count for that bin divided by the total count of all bins.

The ratio of energy to Shannon entropy for each wavelet over the ensemble was summed to determine the optimum wavelet family. Bootstrap resampling at the individual level (to account for between-eye correlations) was performed 1000 times initialized by a fixed seed to determine the 95% confidence intervals. The wavelet selection process used the input feature matrix only and not the outcome measure (in a similar fashion to principal components analysis), and thus did not require cross-validation. The optimum wavelet was used to extract features from the traces for subsequent predictive modeling. In this study, the 16 wavelet coefficients of the sixth decomposition level (center frequency of 32 Hz) were used for both the wavelet selection and the subsequent predictive modeling.

Matching Pursuit

The matching pursuit calculations were performed in MATLAB 2019b (MathWorks, Natick, MA) using the wavelet toolbox. Figure 4 illustrates a sample MP decomposition of the waveform presented in Figure 2 with the 12 atoms of highest importance shown.

Figure 4A shows the atoms themselves and Figure 4B shows each atom multiplied by the coefficient. Summing all of the traces in Figure 4B would return the original signal.

Dictionaries were created in MATLAB for the matching pursuit algorithm. A length of 1024 was specified via the wmpdictionary function, and, for each wavelet packet family, dictionaries were created across a range of orders and vanishing moments. Each dictionary had a size of 1024 × 1024, representing the length of the signal and the number of atoms created. Dictionaries were created from the following wavelet packets: Coiflet, Daubechies, Meyer, Fejer–Korovkin, and Symlet. Like the DWT, these resulting dictionaries had varying properties. For example, the Feyer–Korovkin wavelet packet generates more concentrated wavelet packets with less leakage of high-frequency noise.[51] Optimization of the dictionary to the ensemble was performed over the choice of generating wavelet, the order, and the number of vanishing moments. For each dictionary, a smaller subdictionary of 25 atoms was selected as the top 25 atoms used within each full dictionary. The subdictionaries were compared to one another by decomposing and reconstructing each signal and finding the total root mean square error (RMSE) of the residuals over the whole ensemble. Reconstruction was performed with the wmpalg function using the orthogonal matching

pursuits option and setting the number of iterations to 25 (i.e., the size of the smaller dictionary). The function returns the fit and the residual and the latter was used to calculate the RMSE for each fit. The best dictionary was considered that with the smallest RMSE. Bootstrap resampling was performed again in the same manner as for DWT to determine the 95% confidence intervals for the RMSE. As for the DWT, the outcome measure was not used for this step, so cross-validation was not required. The inputs to the MP model therefore consisted of 25 features corresponding to the coefficients for the atoms in the dictionary.

Predictive Modeling

To examine the value of time–frequency features from the ERG for predicting glaucoma severity based on the eRGC counts, predictive models utilizing the amplitude markers (a-wave, b-wave, i-wave, PhNR1, and PhNR2) were used as a base-case scenario for comparisons, given that we previously demonstrated that the use of this set of amplitude markers improved the prediction of glaucoma severity compared with the PhNR measure alone.[21] The performance of the base-case amplitude marker models was compared with that of models using these features plus additional DWT and/or MP features.

Two types of predictive models were fitted for each of the sets of features extracted from the ERGs. The models tested were a simple linear model and a multivariate adaptive regression spline (MARS) model,[52] an interpretable type of machine learning model that, as we have previously shown, improves the prediction of glaucoma severity with the ERG.[21] The outcome measure of a MARS model is a linear sum of piecewise linear functions. The Caret[53] package (version 6.0-86) in R was used for model fitting and tuning. For both linear and MARS models, overfitting was avoided by using 10-fold cross-validation. For the MARS models, the degree was set to 1 (that is, with no interaction terms), and the maximum number of terms was set to 40. MARS models were fitted using the Earth 5.3.0 package in R.[54]

For each of the tuned "final models," the performance in predicting the eRGC counts was evaluated by the proportion of variance of the eRGC counts explained (R^2) value. Each model was compared to the base case of the amplitude-based marker models. Comparisons were also made between linear and MARS models. The significance of difference in the prediction performance was determined by bootstrapped resampling ($n = 1000$ resamples with a fixed seed for the session) at the participant level.

Results

A total of 103 eyes with glaucoma from 55 participants were included in this study, and their characteristics are shown in Table 1. On the basis of the MD, 12 eyes (11.6%) had severe glaucoma (MD < -12 dB) and 16 eyes (15.5%) had moderate glaucoma (-12 dB $<$ MD < -6 dB).

Discrete Wavelet Transform

Figure 5 shows the energy to entropy ratio for all the discrete wavelets used in the study. A higher ratio indicates a more optimum wavelet. With this metric for this set of traces, the Coiflet 8 was the best wavelet for the decomposition with an energy-to-entropy ratio of 9534 (SD = 2371) Using the Dunnett test for post hoc pairwise comparisons,[55] this wavelet was significantly better than all others ($P < 0.01$).

Matching Pursuit

The results for the matching pursuit dictionary selection are shown in Figure 6. Optimization was undertaken across mother wavelet, order of wavelet, and number of vanishing moments. The best overall dictionary was created by the symlet of order 6 (wpsym6) with six vanishing moments (VMs) having an RMSE of 33.5 nV (SD = 16.6 nV) Using the Dunnett test for post hoc pairwise comparisons, this dictionary was found to be significantly better ($P < 0.01$) than all other dictionaries except symlets of order 6 with VM 7 ($P = 0.24$) and order 8 with VMs 7 and 8 ($P = 0.29$ and $P = 1.0$, respectively), as well as Coiflet

Table 1. Characteristics of the Individuals and Eyes With Glaucoma in the Study

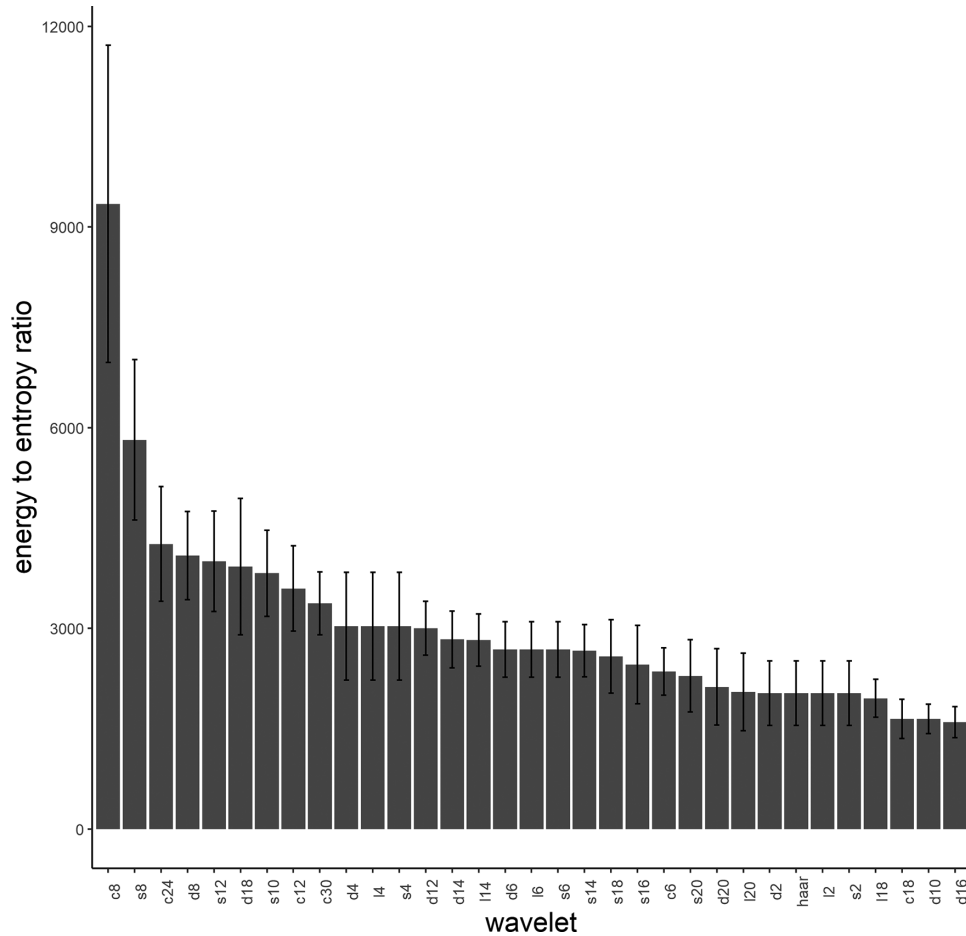| Characteristic	
Individuals (*n* = 55)	
Age (y), median (IQR)	75 (66–80)
Gender (female), *n* (%)	21 (38)
Diabetes (present), *n* (%)	7 (13)
Hypertension (present), *n* (%)	35 (64)
Eyes (*n* = 103), median (IQR)	
Refraction sphere (D)	0.00 (−1.00 to 0.50)
Visual acuity (logMAR)	0.0 (−0.1 to 0.1)
IOP (mmHg)	15.0 (12.0 to 16.0)
Mean deviation (dB)	−2.5 (−5.9 to −0.5)
RNFL thickness (μm)	73 (63 to 83)
eRGC (1000s)	601 (470 to 753)

IQR, interquartile range.

Figure 5. Energy-to-entropy ratio for all of the wavelets in descending order. Wavelets are identified by family and length. C, Coiflet; s, symlet; d, Daubechies; l, best localized. Higher values indicate more optimum discrete wavelets for the decomposition. The *error bars* represent the 95% confidence intervals determined by bootstrap resampling.

dictionaries with order 4 VM 6 ($P = 0.87$) and order 3 VM 7 ($P = 1.0$).

Predictive Modeling

Table 2 shows the summary of model performance for the base-case amplitude marker model compared to those with additional time–frequency features for both the linear and MARS models. Compared to a model using the ERG amplitude markers alone ($R^2 = 0.21$ and $R^2 = 0.34$ for the linear and MARS models, respectively), the models that additionally included the time–frequency features to the amplitude markers significantly improved the predictive performance of the eRGC counts ($R^2 \geq 0.41$ and $R^2 \geq 0.53$ for the linear and MARS models, respectively; $P \leq 0.011$) (Table 2). Pairwise differences among models 2, 3, and 4 did not reach significance within

the model type (linear or MARS $P > 0.05$ for all comparisons).

Discussion

The use of electrophysiological tests to assess glaucoma is appealing in that it can be an objective measure of retinal function. The two established techniques are the PERG and the PhNR. The PERG is elicited with a patterned stimulus in which the pattern changes but the overall luminance remains constant over time.[56] Studies have shown changes in the amplitude markers of the transient[57] and steady-state[58] PERG. The PhNR elicited with a Ganzfeld dome has the advantage over the PERG of not requiring clear optics or refractive correction and may be technically easier to collect.[17]
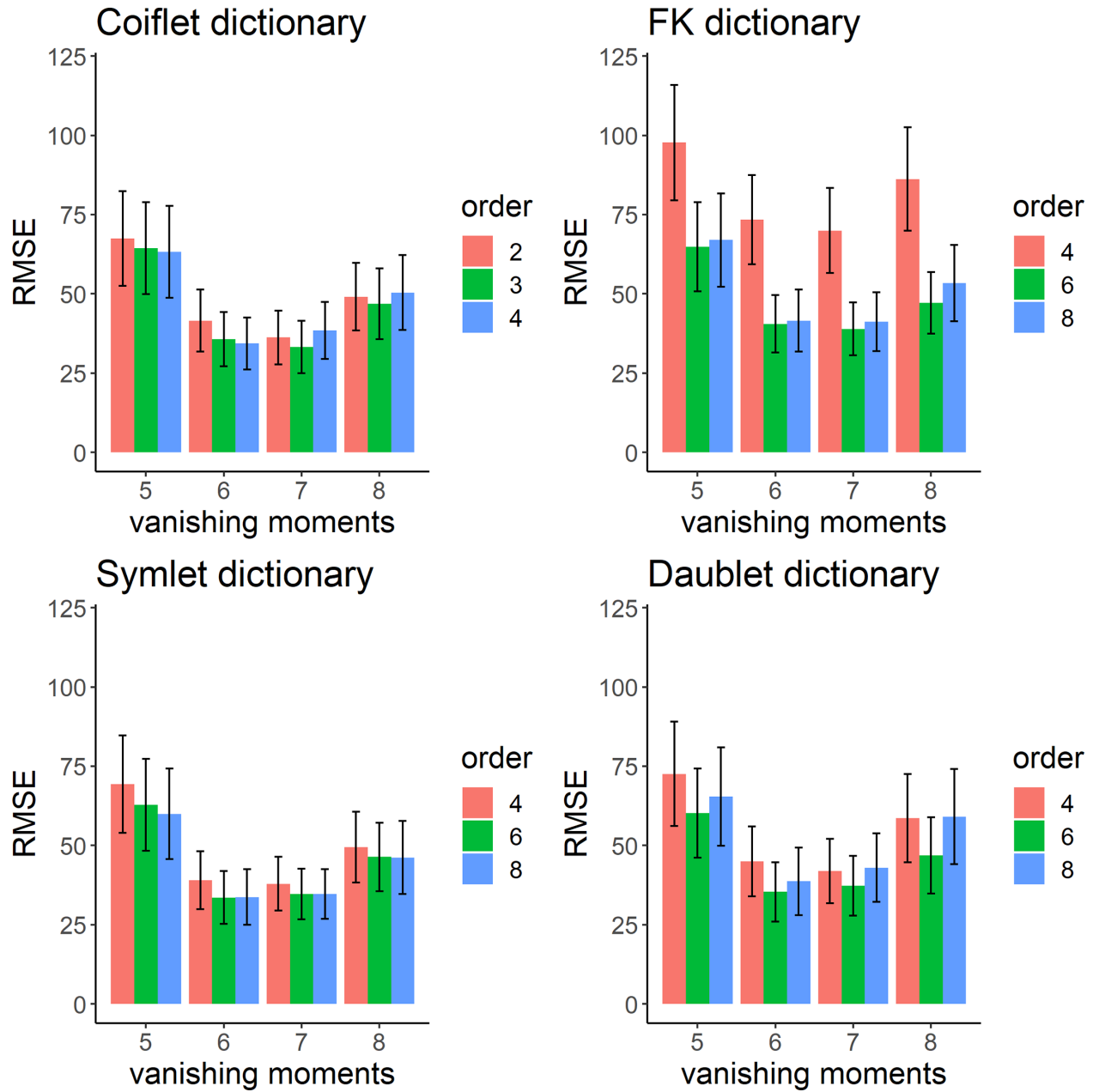
Figure 6. Matching pursuit dictionary optimization. FK, Fejer–Korovkin wavelet. The bar graphs show the residual sum of squares from reconstruction of the ensemble traces for different mother wavelet packets (by panel), vanishing moments (abscissa), and order of wavelet packet (by *color*). *Error bars*: 95% confidence intervals.

This study, which collected electroretinograms with a PhNR protocol, demonstrated that features from time–frequency analyses of the photopic ERG—when using either the DWT or MP—significantly improved the prediction of glaucoma severity when added to amplitude markers evaluated in the time-domain signal. These findings underscore how there is more information in the ERG about RGC dysfunction that could be uncovered using time–frequency analyses, which could potentially aid in the prediction of future RGC loss in glaucoma.

The ERG is a mass signal response, the sum of many different generating components from the inner and outer retina. Feedback loops are well described within the retina,[24,59,60] and RGC discharge spike trains have been shown to spontaneously oscillate in a variety of species.[61] These oscillations and the characteristic waveforms could have a distinctive time–frequency pattern; thus, it is possible that RGC dysfunction occurring in glaucoma could be identifiable with time–frequency analyses of the ERG. Our findings that the combination of the ERG time-domain

Table 2. Performance of Linear and MARS Models in Predicting eRGC From Time and Time–Frequency Features Derived From ERGs

	Linear		MARS		
	R^2	P^a	R^2	P^a	P, Linear vs. MARS
Model 1: Markers	0.21 (0.07)	—	0.34 (0.06)	—	0.004
Model 2: DWT + markers	0.41 (0.08)[b]	0.001	0.53 (0.07)[b]	0.011	0.055
Model 3: MP + markers	0.43 (0.08)[b]	0.001	0.63 (0.08)[b]	<0.001	0.002
Model 4: DWT + MP + markers	0.50 (0.09)[b]	0.001	0.63 (0.07)[b]	0.001	<0.001

Model 1 was informed by the amplitudes of the a-wave, b-wave, i-wave, PhNR1, and PhNR2. Numbers in parentheses indicate standard deviation from the bootstrap resampling.

[a]When compared to model 1.

[b]Not significantly different at $P < 0.05$ for pairwise comparisons among models 2, 3, and 4 for the linear and MARS models separately.

amplitude markers and time–frequency features improved the prediction of glaucoma severity is consistent with observations seen in other fields. One previous study showed that the combination of time and time–frequency features from the electroencephalogram improved the prediction of the error rate for a behavioral task.[62] Another study demonstrated that the addition of time–frequency features to the time-domain features also improved the prediction of sudden cardiac death from heart rate variability data from the electrocardiogram.[63]

The findings of this study build upon our previous work, further reinforcing how there is substantially more information present in the photopic ERG beyond the PhNR amplitude or ratio of PhNR to b-wave alone,[21] which currently remain the primary recommended measures for assessing RGC function on the ERG.[11] However, the improved prediction of glaucoma severity at cross-section when incorporating features from time–frequency analyses does not guarantee its improved utility for the clinically important task of predicting RGC loss in glaucoma, which remains a significant challenge.[64,65] The findings in this study provide further evidence to support the conduct of future longitudinal studies to explore whether the ERG could provide added clinical utility for this purpose. Furthermore, recovery of the PhNR in some eyes with glaucoma following IOP lowering and nicotinamide has been previously described,[18,19] and it may be that time–frequency analysis may also show such functional recovery better than amplitude measurements of the PhNR alone. The ERG as a measure of function rather than structure may not be able to distinguish between reversible and irreversible loss of RGC function. However reversible RGC dysfunction could potentially be identified through evaluating the discordance between the observed and expected RGC function based on estimates of RGC loss (such as

through the eRGC counts parameter in this study), which could also be examined in future longitudinal studies. Further exploration of the nature of feedback and feedforward pathways could be done with hierarchical decomposition analysis.[66] This technique uses multiple electrodes to decompose a set of signals into their constituent sources. The technique assumes that there is a dominant generator with subsequent generators dependent upon the dominant one—hence, the hierarchy. This technique may become possible with multi-electrode contact lens electrodes such as those that have been used in the rat.[67]

Limitations of this study include the relatively small sample size and the limited range of glaucoma severity, but the cohort nonetheless enabled the demonstration of the significant added value of features from time–frequency analyses. We used the analysis of ensemble averages with timing relative to the peak of the b-wave rather than relative to the flash onset to account for latency and phase variations among individuals. This is an alternative technique to the local wavelet maximum technique used by Gauvin and colleagues[68] and does have the advantage that the decomposition is invertible. This technique results in the loss of timing information, although timing features are generally not used for analysis of the PhNR. Both the MP and the DWT optimization were performed on glaucoma participants alone, and it may be that inclusion of eyes without glaucoma could yield a different result. Construction of a mixed cohort for test optimization would require knowledge of the prior probability of the existence and extent of glaucoma in an eye undergoing the test. Such an approach was beyond the scope of this study. Although in our study better performance was obtained with the MP technique, the DWT is more intuitive, and our DWT methods are easier to replicate by others compared to the MP decomposition, which requires access to our custom dictionary.

In this work, we did not attempt to establish that the electroretinogram can better estimate the glaucoma severity than existing techniques such as the eRGC. To do so would require a ground truth such as histological ganglion cell counts, and even this would not necessarily reveal the functional state of the RGCs. We have, however, shown that conventional time-domain amplitude analysis techniques might not be extracting all of the useful information available from the ERG in glaucoma.

Conclusions

This study demonstrated that features extracted from the ERG using time–frequency analyses yield additional predictive information about the severity of glaucoma. This is biologically plausible given that the ERG is made up of a sequence of different processes with different frequency responses that can become impaired in glaucoma. These findings encourage future longitudinal studies to understand whether this technique could be clinically useful for predicting glaucoma progression.

Acknowledgments

Disclosure: **M. Sarossy**, None; **J. Crowston**, None; **D. Kumar**, None; **A. Weymouth**, None; **Z. Wu**, None

References

1. Weinreb RN, Aung T, Medeiros FA. The pathophysiology and treatment of glaucoma: a review. *JAMA*. 2014;311:1901–1911.
2. Fry LE, Fahy E, Chrysostomou V, et al. The coma in glaucoma: retinal ganglion cell dysfunction and recovery. *Prog Retin Eye Res*. 2018;65:77–92.
3. Kalesnykas G, Oglesby EN, Zack DJ, et al. Retinal ganglion cell morphology after optic nerve crush and experimental glaucoma. *Invest Ophthalmol Vis Sci*. 2012;53:3847–3857.
4. Della Santina L, Inman DM, Lupien CB, Horner PJ, Wong RO. Differential progression of structural and functional alterations in distinct retinal ganglion cell types in a mouse model of glaucoma. *J Neurosci*. 2013;33:17444–17457.
5. Risner ML, Pasini S, Cooper ML, Lambert WS, Calkins DJ. Axogenic mechanism enhances retinal ganglion cell excitability during early progression in glaucoma. *Proc Natl Acad Sci USA*. 2018;115:E2393–E2402.
6. Calkins DJ. Adaptive responses to neurodegenerative stress in glaucoma. *Prog Retin Eye Res*. 2021;84:100953.
7. Weber AJ, Harman CD. Structure–function relations of parasol cells in the normal and glaucomatous primate retina. *Invest Ophthalmol Vis Sci*. 2005;46:3197–3207.
8. Tham Y-C, Li X, Wong TY, Quigley HA, Aung T, Cheng C-Y. Global prevalence of glaucoma and projections of glaucoma burden through 2040: a systematic review and meta-analysis. *Ophthalmology*. 2014;121:2081–2090.
9. Banitt MR, Ventura LM, Feuer WJ, et al. Progressive loss of retinal ganglion cell function precedes structural loss by several years in glaucoma suspects. *Invest Ophthalmol Vis Sci*. 2013;54:2346–2352.
10. Liu HH, He Z, Nguyen CT, Vingrys AJ, Bui BV. Reversal of functional loss in a rat model of chronic intraocular pressure elevation. *Ophthalmic Physiol Opt*. 2017;37:71–81.
11. Frishman L, Sustar M, Kremers J, et al. ISCEV extended protocol for the photopic negative response (PhNR) of the full-field electroretinogram. *Doc Ophthalmol*. 2018;136:207–211.
12. Viswanathan S, Frishman LJ, Robson JG, Walters JW. The photopic negative response of the flash electroretinogram in primary open angle glaucoma. *Invest Ophthalmol Vis Sci*. 2001;42:514–522.
13. Machida S, Gotoh Y, Toba Y, Ohtaki A, Kaneko M, Kurosaka D. Correlation between photopic negative response and retinal nerve fiber layer thickness and optic disc topography in glaucomatous eyes. *Invest Ophthalmol Vis Sci*. 2008;49:2201–2207.
14. North RV, Jones AL, Drasdo N, Wild JM, Morgan JE. Electrophysiological evidence of early functional damage in glaucoma and ocular hypertension. *Invest Ophthalmol Vis Sci*. 2010;51:1216–1222.
15. Nakamura H, Hangai M, Mori S, Hirose F, Yoshimura N. Hemispherical focal macular photopic negative response and macular inner retinal thickness in open-angle glaucoma. *Am J Ophthalmol*. 2011;151:494–506.e1.
16. Machida S, Kaneko M, Kurosaka D. Regional variations in correlation between photopic

negative response of focal electoretinograms and ganglion cell complex in glaucoma. *Curr Eye Res*. 2015;40:439–449.

17. Preiser D, Lagreze WA, Bach M, Poloschek CM. Photopic negative response versus pattern electroretinogram in early glaucoma. *Invest Ophthalmol Vis Sci*. 2013;54:1182–1191.

18. Tang J, Hui F, Hadoux X, et al. Short-term changes in the photopic negative response following intraocular pressure lowering in glaucoma. *Invest Ophthalmol Vis Sci*. 2020;61:16.

19. Hui F, Tang J, Williams PA, et al. Improvement in inner retinal function in glaucoma with nicotinamide (vitamin B3) supplementation: a crossover randomized clinical trial. *Clin Exp Ophthalmol*. 2020;48:903–914.

20. Rosolen SG, Rigaudière F, LeGargasson JF, et al. Comparing the photopic ERG i-wave in different species. *Vet Ophthalmol*. 2004;7:189–192.

21. Sarossy M, Crowston J, Kumar D, Weymouth A, Wu Z. Prediction of glaucoma severity using parameters from the electroretinogram. *Sci Rep*. 2021;11:23886.

22. Robson JG, Frishman LJ. Dissecting the dark-adapted electroretinogram. *Doc Ophthalmol*. 1998;95:187–215.

23. Sieving PA, Murayama K, Naarendorp F. Push–pull model of the primate photopic electroretinogram: a role for hyperpolarizing neurons in shaping the b-wave. *Vis Neurosci*. 1994;11:519–532.

24. Crook JD, Manookin MB, Packer OS, Dacey DM. Horizontal cell feedback without cone type-selective inhibition mediates "red–green" color opponency in midget ganglion cells of the primate retina. *J Neurosci*. 2011;31:1762–1772.

25. Dong C-J, Agey P, Hare WA. Origins of the electroretinogram oscillatory potentials in the rabbit retina. *Vis Neurosci*. 2004;21:533.

26. Puller C, Haverkamp S, Neitz M, Neitz J. Synaptic elements for GABAergic feed-forward signaling between HII horizontal cells and blue cone bipolar cells are enriched beneath primate S-cones. *PLoS One*. 2014;9:e88963.

27. Morlet J. Sampling theory and wave propagation. In: Chen CH, ed. *Issues in Acoustic Signal—Image Processing and Recognition*. Berlin: Springer; 1983:233–261.

28. Goupillaud P, Grossmann A, Morlet J. Cycle-octave and related transforms in seismic signal analysis. *Geoexploration*. 1984;23:85–102.

29. Hassankarimi H, Noori SMR, Jafarzadehpour E, Yazdani S, Radinmehr F. Analysis of pattern electroretinogram signals of early primary open-angle glaucoma in discrete wavelet transform coefficients domain. *Int Ophthalmol*. 2019;39:2373–2383.

30. Miguel-Jiménez J, Boquete L, Ortega S, Rodriguez-Ascariz J, Blanco R. Glaucoma detection by wavelet-based analysis of the global flash multifocal electroretinogram. *Med Eng Phys*. 2010;32:617–622.

31. Kundra H, Park JC, McAnany JJ. Comparison of photopic negative response measurements in the time and time–frequency domains. *Doc Ophthalmol*. 2016;133:91–98.

32. Daubechies I. *Ten Lectures on Wavelets*. Philadelphia, PA: Society for Industrial and Applied Mathematics; 1992.

33. Forte JD, Bui BV, Vingrys AJ. Wavelet analysis reveals dynamics of rat oscillatory potentials. *J Neurosci Methods*. 2008;169:191–200.

34. Behbahani S, Ramezani A, Karimi Moridani M, Sabbaghi H. Time–frequency analysis of photopic negative response in CRVO patients. *Semin Ophthalmol*. 2020;35:187–193.

35. Mallat SG. A theory for multiresolution signal decomposition: the wavelet representation. *IEEE Trans Pattern Anal Mach Intell*. 1989;11:674–693.

36. Daubechies I. Orthonormal bases of compactly supported wavelets. *Commun Pure Appl Math*. 1988;41:909–996.

37. Kumar P, Foufoula-Georgiou E. Wavelet analysis for geophysical applications. *Rev Geophys*. 1997;35:385–412.

38. Gauvin M, Sustar M, Little JM, Brecelj J, Lina J-M, Lachapelle P. Quantifying the ON and OFF contributions to the flash ERG with the discrete wavelet transform. *Transl Vis Sci Technol*. 2017;6:3.

39. Constable PA, Marmolejo-Ramos F, Gauthier M, Lee IO, Skuse DH, Thompson DA. Discrete wavelet transform analysis of the electroretinogram in autism spectrum disorder and attention deficit hyperactivity disorder. *Front Neurosci*. 2022;16:890461.

40. Mallat S, Zhang Z. *Matching Pursuit with Time–Frequency Dictionaries*. New York: Courant Institute of Mathematical Sciences; 1993.

41. Hsu P-H. Feature extraction of hyperspectral images using wavelet and matching pursuit. *ISPRS J Photogramm Remote Sens*. 2007;62:78–92.

42. Zarei A, Asl BM. Automatic seizure detection using orthogonal matching pursuit, discrete wavelet transform, and entropy based features of EEG signals. *Comput Biol Med*. 2021;131:104250.

43. Medeiros FA, Lisboa R, Weinreb RN, Girkin CA, Liebmann JM, Zangwill LM. A combined index of structure and function for staging glaucomatous damage. *Arch Ophthalmol*. 2012;130:1107–1116.

44. Harwerth R, Wheat J, Fredette M, Anderson D. Linking structure and function in glaucoma. *Prog Retin Eye Res*. 2010;29:249–271.

45. Wu Y, Cun Q, Tao Y, et al. Evaluation of macular and retinal ganglion cell count estimates for detecting and staging glaucoma. *Front Med*. 2021;8:740761.

46. Wakili N, Horn FK, Jünemann AG, et al. The photopic negative response of the blue-on-yellow flash-electroretinogram in glaucomas and normal subjects. *Doc Ophthalmol*. 2008;117:147–154.

47. DB Percival, Walden AT. *Wavelet Methods for Time Series Analysis*. Cambridge, UK: Cambridge University Press; 2008.

48. Adamo F, Andria G, Attivissimo F, Lanzolla AML, Spadavecchia M. A comparative study on mother wavelet selection in ultrasound image denoising. *Measurement*. 2013;46:2447–2456.

49. Shigueoka LS, de Vasconcellos JPC, Schimiti RB, et al. Automated algorithms combining structure and function outperform general ophthalmologists in diagnosing glaucoma. *PLoS One*. 2018;13:e0207784.

50. Zhang Z, Zhang X. A normal law for the plug-in estimator of entropy. *IEEE Trans Inform Theory*. 2011;58:2745–2747.

51. Kadir R, Saha R, Akhter MM, Awal MA, Kadir MI. LDPC coded hybrid discrete cosine transform and Fejér–Korovkin wavelet transform-based SC-FDMA for image communication. *Array*. 2021;12:100107.

52. Friedman JH. Multivariate adaptive regression splines. *Ann Statist*. 1991;19:1–67.

53. Kuhn M. caret: classification and regression training. Available at: https://cran.r-project.org/web/packages/caret/caret.pdf. Accessed September 26, 2022.

54. Milborrow S. earth: multivariate adaptive regression splines. Available at: https://cran.r-project.org/web/packages/earth/earth.pdf. Accessed September 26, 2022.

55. Vizzeri G, Tafreshi A, Weinreb RN, Bowd C. Effect of operator and optical defocus on the variability of pattern electroretinogram optimized for glaucoma detection (PERGLA). *J Glaucoma*. 2010;19:77.

56. Bach M, Brigell MG, Hawlina M, et al. ISCEV standard for clinical pattern electroretinography (PERG): 2012 update. *Doc Ophthalmol*. 2013;126:1–7.

57. Parisi V, Manni G, Centofanti M, Gandolfi SA, Olzi D, Bucci MG. Correlation between optical coherence tomography, pattern electroretinogram, and visual evoked potentials in open-angle glaucoma patients. *Ophthalmology*. 2001;108:905–912.

58. Bach M, Unsoeld AS, Philippin H, et al. Pattern ERG as an early glaucoma indicator in ocular hypertension: a long-term, prospective study. *Invest Ophthalmol Vis Sci*. 2006;47:4881–4887.

59. Purpura K, Tranchina D, Kaplan E, Shapley RM. Light adaptation in the primate retina: analysis of changes in gain and dynamics of monkey retinal ganglion cells. *Vis Neurosci*. 1990;4:75–93.

60. Davenport CM, Detwiler PB, Dacey DM. Effects of pH buffering on horizontal and ganglion cell light responses in primate retina: evidence for the proton hypothesis of surround formation. *J Neurosci*. 2008;28:456–464.

61. Neuenschwander S, Castelo-Branco M, Singer W. Synchronous oscillations in the cat retina. *Vision Res*. 1999;39:2485–2497.

62. Munneke G-J, Nap TS, Schippers EE, Cohen MX. A statistical comparison of EEG time- and time–frequency domain representations of error processing. *Brain Res*. 2015;1618:222–230.

63. Ebrahimzadeh E, Pooyan M, Bijar A. A novel approach to predict sudden cardiac death (SCD) using nonlinear and time–frequency analyses from HRV signals. *PLoS One*. 2014;9:e81896.

64. Ernest PJ, Schouten JS, Beckers HJ, Hendrikse F, Prins MH, Webers CA. Prediction of glaucomatous visual field progression using baseline clinical data. *J Glaucoma*. 2016;25:228–235.

65. De Moraes CG, Sehi M, Greenfield DS, Chung YS, Ritch R, Liebmann JM. A validated risk calculator to assess risk and rate of visual field progression in treated glaucoma patients. *Invest Ophthalmol Vis Sci*. 2012;53:2702–2707.

66. Repucci M, Schiff N, Victor J. General strategy for hierarchical decomposition of multivariate time series: implications for temporal lobe seizures. *Ann Biomed Eng*. 2001;29:1135–1149.

67. Derafshi Z, Kunzer BE, Mugler EM, et al. Corneal potential maps measured with multi-electrode electroretinography in rat eyes with experimental lesions. *Invest Ophthalmol Vis Sci*. 2017;58:2863–2873.

68. Gauvin M, Little JM, Lina J-M, Lachapelle P. Functional decomposition of the human ERG based on the discrete wavelet transform. *J Vis*. 2015;15:14.